frontiers | Frontiers in Physics

TYPE Original Research
PUBLISHED 15 January 2026
DOI 10.3389/fphy.2025.1740296

OPEN ACCESS

EDITED BY
Mauro Menichelli,
Istituto Nazionale di Fisica Nucleare di Perugia, Italy

REVIEWED BY
Belafrites Abdelfettah,
University of Jijel, Algeria
Gebi Tuku,
Mizan Tepi University, Ethiopia

*CORRESPONDENCE
Mashinga J. Mvelase,
emjay.mvelase@gmail.com

RECEIVED 05 November 2025
REVISED 16 December 2025
ACCEPTED 18 December 2025
PUBLISHED 15 January 2026

CITATION
Mvelase MJ, Ntshangase SS, Majola SNT, Kheswa BV, Masiteng PL and Maleka PP (2026) The study of radiation contamination in roodepoort gold mine tailings using HPGe gamma spectroscopy.
Front. Phys. 13:1740296.
doi: 10.3389/fphy.2025.1740296

The study of radiation contamination in roodepoort gold mine tailings using HPGe gamma spectroscopy

Mashinga J. Mvelase[1,2]*, Sifiso S. Ntshangase[1], Siyabonga N. T. Majola[2], Bonginkosi V. Kheswa[2], Paulus L. Masiteng[2] and Peane P. Maleka[3,4]

[1]Department of Physics, University of Zululand, KwaDlangezwa, South Africa, [2]Department of Physics, University of Johannesburg, Doornfontein, South Africa, [3]SSC Laboratory, iThemba Laboratory for Accelerator Based Sciences, Somerset West, South Africa, [4]University of the Western Cape, Bellville, South Africa

In this study, a coaxial HPGe high-resolution γ-detector was used to measure the γ-signals in soil samples collected from the Roodepoort Gold Tailings. There have been complaints about dust from the gold tailings, and the study aims to determine the level of contamination. The activity concentration of ^{238}U ranged from 132.88 ± 4.68 to 1,421.46 ± 13.38, with a mean of 464.96 ± 2.08 Bq/kg. The activity concentration of ^{226}Ra ranged from 130.19 ± 4.48 to 1,359.27 ± 13.83, with a mean of 425.28 ± 8.02 Bq/kg. The range of ^{232}Th was from 5.27 ± 0.67 to 19.37 ± 1.98, with a mean of 11.20 ± 1.03 Bq/kg, and ^{40}K activity ranged from 65.23 ± 15.29 to 264.11 ± 25.66, with a mean of 127.50 ± 21.85 Bq/kg. The findings showed that ^{238}U and ^{226}Ra activities exceeded the global average of 35 Bq/kg, while ^{232}Th and ^{40}K were below their respective limits. The radiological hazard indices exceeded recommended limits, making the tailings soil completely unsuitable for use as building materials, as this may have deleterious health effects on residents in the future.

KEYWORDS

AEDE, ELCR, HPGe γ - spectroscopy, radioactivity, radiological health hazards

1 Introduction

Since the formation of the Earth, natural background ionizing radiation has always emanated from the decays of ^{238}U, ^{232}Th, and ^{40}K, which are present in the environment [1, 2]. Two isotopes make up most of the natural uranium found in Earth's crust: ^{238}U, which accounts for 99.3 % and ^{235}U, which accounts for approximately 0.7% [3, 4]. Radioactivity is significant in the mining and processing of ores other than uranium. These activities result in exposure to naturally occurring radioactive materials (NORM). Radiological exposures associated with radioactivity, such as absorbed dose rate, annual effective dose rate, and annual gonadal dose rate, should be evaluated. Most background ionising radiation originates from the decay of the ^{238}U decay series, the ^{232}Th decay series, and the non-series ^{40}K [4–6]. In Soweto, environmental radioactivity originates from mining tailings, and radiation is transported as dust by the wind to distant locations, so no one is spared from radiation contamination.

Radiation affects the human body externally through γ-radiation and internally through α-radiation, which arises from inhaling dust and radon (^{222}Rn) gas. Radon gas is the parent

nucleus of both ^{218}Po and ^{214}Po, which are alpha emitters. Alpha particles can damage DNA by imparting a high density of ionizations due to their high linear energy transfer [7]. High linear energy transfer (LET) single hits can generate highly reactive oxygen species capable of inducing cellular damage by direct reaction with biological molecules [8], as well as nitrogen radicals, which may cause significant DNA damage. High LET radiation is more effective than low LET radiation at inducing cell death, apoptosis, mutation, transformation, carcinogenesis, chromosomal abnormalities, and chromosomal instability [9]. The highly reactive oxygen species (ROS) produced by high LET radiation consequently damage various cell components, such as lipids, proteins, and nucleic acids, resulting in several chronic and degenerative conditions, including ageing, dementia, kidney, cardiovascular and neurodegenerative diseases, cancer, respiratory disorders, rheumatoid arthritis, and other metabolic disorders [10]. Nuclear decays inside the body emit α-, β-, and γ-radiation [11, 12], which can damage DNA through cell ionizations. Alpha particles impart a high density of ionizations along their short path, as they have a high linear energy transfer, leading to DNA damage in human cells and potentially resulting in radiation-induced carcinogenesis [13]. Previous studies have reported that the gold mine tailings in the Witwatersrand Basin have a uranium concentration of 100 mg/kg U_3O_8, which is comparable to or higher than the concentrations of uranium mine tailings in Namibia, ranging from 45.9 ± 3.0 to 1752.1 ± 17.5 Bq/kg for ^{238}U [14, 15].

The mining sector has had both positive and negative effects on the South African economy and gross domestic product (GDP) [16]. South Africa is endowed with numerous mineral resources, particularly metals, coal, and gold, with exploration beginning in the late 1800s [4] and mining commencing in 1886 [17]. Extensive mining activity has occurred, bringing soils and rocks that would otherwise have remained underground to the surface. These activities have left behind mountains of pollution known as mining tailings. Gold tailings are a source of dust, especially during the dry and windy season, due to their proximity to residential areas, affecting thousands of impoverished township residents and causing numerous health issues [18–20]. Inhaling toxic metals trapped in radioactive dust particles can cause various lung diseases [16]. In the context of climate change, gold tailings are even more hazardous due to unpredictable weather patterns and heavy rains that may cause overflow, allowing pollution to reach human settlements. Toxic metals such as As, Cr, and Ni, and radioactive metals such as ^{238}U, ^{232}Th, and ^{40}K in tailings pose a synergistic health risk to residents [4]. Knowledge of the distribution of geogenic and anthropogenic radionuclides is recommended for assessing and managing public health risks and should inform any environmental interventions [21].

Most written reports are based primarily on the work of community activists and community-based non-governmental organizations (NGOs) campaigning against mining companies that have left pollution unaddressed. This study aims to measure radioactivity in gold mine tailings, which has been less frequently reported, providing valuable information on radioactivity concentrations. Based on the results, the corresponding probabilistic health risk will be calculated.

2 Materials and methods

2.1 Geology and climate of the study area

The study site has a subtropical highland climate with a warm, wet summer [22]. These tailings are from abandoned old gold mines. The research area's land is mostly utilized for residential development, with very little employed for gold mining [22, 23]. The gold-bearing conglomerates in the sedimentary layers of the West Rand mining area consist of 10–30 % phyllosilicates and 70–90 % quartz SiO_2. Uraninite UO_2, brannerite $UO_3Ti_2O_4$, arsenopyrite (FeAsS), cobaltite (CoAsS), galena (PbS), pyrrhotite (FeS), gersdorfite (NiAsS), and chromite $FeCr_2O_4$, sericite, $KAl_2AlSi_3O_{10}(OH)_2$, and minor minerals such as rutile TiO_2, pyrite FeS_2, chromite $FeCr_2O_4$, and uraninite UO_2 make up the bulk of the phyllosilicates [24, 25]. The West Rand Group, mainly composed of quartzite and shale, forms the sedimentary base. The Central Rand Group is characterized by quartzite and conglomerate, particularly gold-bearing conglomerates in its lower section, which are associated with basin-wide unconformities [26]. The highlands have long, hot summers that generally last from October to March and short, cold winters that last from June to August. Most of the annual rainfall, which ranges from 600 to 732 mm, falls during the summer months. Strong storms are frequent from October to March, and the average annual temperature is 16 °C [25].

2.2 Sample collection and preparation

Soil samples were collected from the gold mine tailings in Roodepoort, located at 26°10′46″S 27°52′03″E, and stored in plastic zipper bags labelled RDP. The study site has residential areas, businesses, and additional mine tailings in its vicinity, as shown in Figure 1. The samples were placed in polypropylene Marinelli beakers of known weight after being oven-dried at 105 °C, crushed, pulverized, and sieved to remove uncrushed stones and organic matter.

To achieve secular equilibrium between the gamma emitters in the ^{238}U series (primarily ^{226}Ra, ^{214}Bi, and ^{214}Pb) and the ^{232}Th series (^{228}Ra measured by ^{228}Ac, and ^{228}Th measured by ^{208}Tl), white silicone was applied between the lid and brim of Marinelli beakers to prevent radon leakage, and the beakers were hermetically sealed for 42 days before γ - spectroscopic analysis, as shown in Figure 2. The gross weights were measured, and the difference between the empty and gross weights gave the sample weights. Most of these sample weights averaged approximately 0.250 kg. The prepared gold tailings soil samples are now in Marinelli beakers, where they are kept until they reach secular equilibrium. They will then remain sealed and analysed at a later stage, as shown in Figure 2.

2.3 Analysis of soil samples

Gamma spectroscopic analysis of the natural radioactivity (^{238}U, ^{232}Th and ^{40}K) in soil was carried out at the Environmental Radiation Laboratory (ERL) at NRF iThemba LABS. The radioactivity was measured using a p-type coaxial Canberra gamma-ray spectrometer detector, optimised for detecting gamma rays at

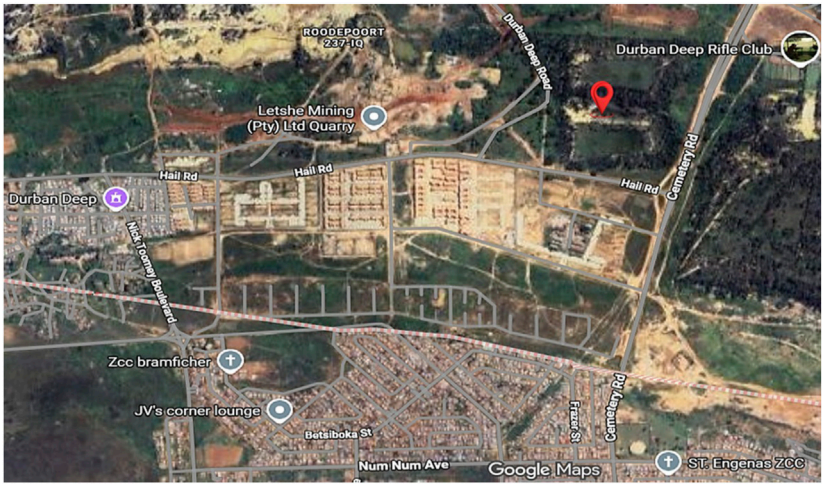

FIGURE 1
The Roodepoort Google Map shows the gold tailings sampling location.

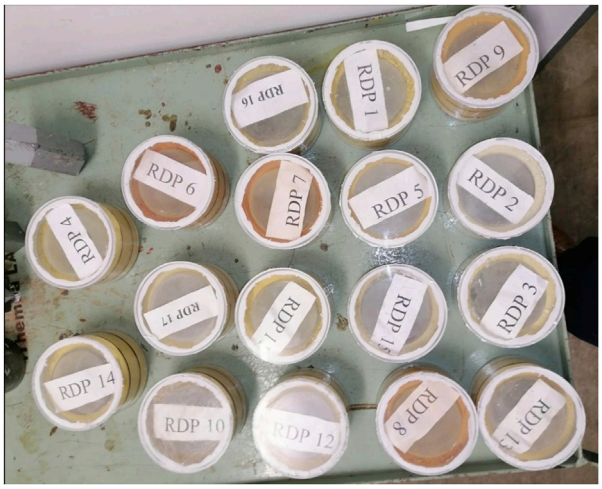

FIGURE 2
The prepared gold tailings soil samples in Marinelli beakers.

low energies up to 2000 keV, Model No. BE2820 SN 8794, with 45% relative efficiency and a resolution of ≤2.00 keV (FWHM) at the 1.33 MeV γ-ray line of ^{60}Co. An electronic data acquisition system (Canberra DSA-1000 digital signal processing (DSP) system), interfaced with a Multichannel Analyzer (MCA) and Canberra Genie 2000 software (version 2.0), was used to acquire a spectrum.

The gamma spectrometry system was calibrated for energy and efficiency using a mixed radionuclide standard covering a wide range of gamma-ray energies (0.060–2.00 MeV) in a 500 ml Marinelli beaker. Both the samples and the background were counted for 25,200 s, and the background count was subtracted from the sample count to give the net count rate. For quality control, calibration for energy and efficiency was performed to maintain measurement quality. After the samples were hermetically sealed for 42 days in their respective Marinelli beakers, secular equilibrium was assumed to have been reached. The 186.22 keV γ-signal was used to quantify ^{226}Ra. The 295.22 keV and 351.93 keV γ-signals for ^{214}Pb and the 609.32 keV, 1,120.29 keV, and 1764.49 keV γ-signals for ^{214}Bi were used to assess the activity concentration of ^{238}U [27–31], while 911.21 keV for ^{228}Ac and 583.1 keV for ^{208}Tl were used for ^{232}Th. The single 1,460 keV γ - signal was used to quantify ^{40}K concentration. The specific γ - signals listed in Table 1 were tracked to measure each radionuclide in the soil samples. The information in the table was sourced from the literature [32, 33].

3 The efficiency and energy calibration curves

When analyzing unknown samples, we rely on gamma spectroscopy; however, before we can use it effectively, we must calibrate the energy scale. To do this, we used several well-known radioactive sources that emit gamma rays at specific energies. These include ^{210}Pb at 45.54 keV, ^{241}Am at 59.5 keV, ^{109}Cd at 88 keV, and ^{57}Co at 122.1 keV, among others. We also use higher-energy sources such as ^{137}Cs (661.65 keV), ^{60}Co (which emits at both 1,173.2 and 1,332.4 keV), and ^{88}Y (1836.1 keV). The emission probabilities for these radionuclides were obtained from previous research papers [34]. The efficiency equation depends on energy, as shown in Equation 1, and has been used in work published by the following authors [35–37]:

$$\varepsilon\left(E_\gamma\right) = \frac{1}{E_\gamma}\sum_{i=1}^{8} a_i\left(\ln\frac{E_\gamma}{E_o}\right)^{i-1} \quad (1)$$

In this equation, E_γ (keV) represents the peak energy of a particular radioisotope of interest, and $E_0 = 1$ keV [38]. The efficiency calibration curve for the HPGe detector was obtained using standard sources at NRF iThemba LABS, Gauteng. As there is a direct relationship between channel number and energy, we can convert our channel readings into energy measurements. The results of both the efficiency and energy calibration curves are shown in Figure 3.

TABLE 1 The data on NORM decay modes showing their specific γ - signals and intensity.

Parent nuclide (NORM)	Daughter Nuclide	Nuclear Half-life	Decay mode (%)	γ-ray energy (keV)	γ-intensity Yield (%)
^{226}Ra	Ra-226	1,602 years	α (94), α (6)	186	3.55
	Pb-214	26.80 min	β (100)	295	19.3
	Pb-214	26.80 min	β (100)	352	37.6
^{238}U	Bi-214	19.90 min	α (0.021)	609	46.1
	Bi-214	19.90 min	β (99.98)	1,120	15.4
	Bi-214	19.90 min	β (99.98)	1764	15.4
^{232}Th	Ac-228	6.15 h	β (100)	911	26.0
	Tl-208	3.05 min	β (100)	583	86.0
^{40}K	Ar-40	1.284×10^9 years	EC (10.7)	1,461	10.7

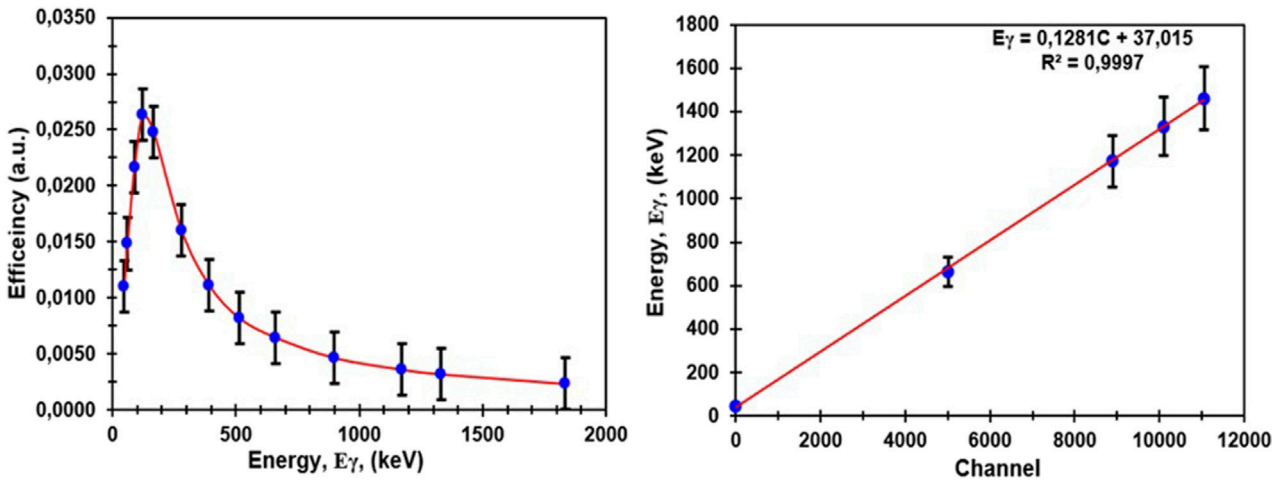

FIGURE 3
Detector efficiency (left) and energy calibration for γ-ray energies (right).

3.1 Minimum detectable activity and error calculations

The background count was conducted using the same geometry as the samples. An empty Marinelli beaker was placed on the detector, as with the sample measurements, and counted for periods similar to those used for the sample counts. The peaks generated from this procedure were subtracted from the corresponding peaks of the samples. In this way, the background count rate was manually subtracted from the measured samples. After determining the background radiation for the radionuclides of interest, the minimum detectable activity (MDA) was calculated using the following Equation 2:

$$MDA\,(Bq/kg) = \frac{2.71 + 4.66\sqrt{B}}{I_\gamma \varepsilon T m} \quad (2)$$

Where MDA (Bq/kg) is the specific activity in a sample, B is the background activity of the sample, ε is the absolute detector efficiency of the specific γ-ray, T is the accumulation time, and m is the mass of the sample in kilograms. I_γ is the emission probability of a specific energy photopeak. Using the background activities, the average MDA for ^{226}Ra is 6.68 Bq/kg at 186.2 keV, 26.1 Bq/kg for ^{40}K at 1,460 keV, and 1.68 Bq/kg for ^{214}Pb at 352 keV.

For specific activity concentration, the error was calculated by taking the square root of the sum of the background and sample readings, then dividing by T, ε, I_γ, and mass m. The resulting value

TABLE 2 The specific activity concentrations of ^{238}U, ^{226}Ra, ^{232}Th and ^{40}K in the tailings.

Gold tailings	Sample ID	Specific activity concentration in roodepoort samples (Bq/kg)			
		^{238}U	^{226}Ra	^{232}Th	^{40}K
Roodepoort	RDP 01	444.81 ± 8.20	397.67 ± 16.6	10.66 ± 0.97	119.52 ± 18.18
	RDP 02	584.28 ± 10.23	470.98 ± 18.73	12.76 ± 1.12	163.42 ± 20.92
	RDP 03	483.32 ± 9.08	413.61 ± 16.26	8.96 ± 0.84	128.92 ± 17.53
	RDP 04	480.67 ± 7.95	393.29 ± 17.04	12.60 ± 1.13	135.19 ± 19.61
	RDP 05	441.44 ± 8.21	367.66 ± 16.82	11.84 ± 1.12	122.94 ± 19.64
	RDP 06	279.51 ± 6.72	347.55 ± 15.788	10.12 ± 0.99	87.83 ± 17.17
	RDP 07	247.96 ± 6,67	296.721 ± 14.26	8.73 ± 0.87	106.15 ± 17.28
	RDP 08	362.03 ± 8.03	276.40 ± 13.06	8.64 ± 0.83	91.18 ± 15.40
	RDP 09	499.35 ± 9.69	472.04 ± 20.27	19.36 ± 1.48	177.19 ± 23.81
	RDP 10	1,421.46 ± 13.38	1,195.80 ± 30.63	18.81 ± 1.42	264.11 ± 25.66
	RDP 11	456.98 ± 7.95	417.81 ± 18.55	14.71 ± 1.23	125.11 ± 20.81
	RDP 12	437.17 ± 8.28	356.985 ± 15.54	10.86 ± 0.97	111.84 ± 17.48
	RDP 13	547.86 ± 10.16	457.89 ± 18.85	10.49 ± 1.05	147.52 ± 20.89
	RDP 14	373.40 ± 8.26	308.16 ± 14.29	8.02 ± 0.80	98.05 ± 16.56
	RDP 15	132.88 ± 4.68	12.02 ± 9.09	5.27 ± 0.67	65.23 ± 15.29
	RDP 16	237.16 ± 6.20	248.18 ± 13.70	6.82 ± 0.79	85.01 ± 17.46
	RDP 17	474.11 ± 8.48	393.29 ± 18.04	11.82 ± 1.19	138.32 ± 21.36
Activity statistics	Min	132.88 ± 6.20	112.02 ± 9.09	5.27 ± 0.67	65.23 ± 15.29
	Max	1,421.46 ± 13.38	1,195.80 ± 30.63	19.37 ± 1.48	264.11 ± 25.66
	Mean	464.96 ± 2.08	407.41 ± 4.23	11.20 ± 1.03	127.50 ± 21.85
	STDev	274.12	222.56	3.76	45.58
	Median	444.81 ± 8.20	393.29 ± 17.04	10.66 ± 0.97	122.94 ± 19.64

was then multiplied by two, as 2σ was used for our measurements. For the other radiological indices, error propagation was applied.

4 Calculations of risk assessment of radionuclides

After calculating the detector efficiency and energy calibration, the samples were subjected to gamma spectroscopic analysis which resulted to the measurement of specific activity concentration. Radiological indices, including Radium Equivalent Ra_{Eq}, Absorbed Dose Rate (ADR), Annual Effective Dose Equivalent (AEDE), Excess Lifetime Cancer Risk (ELCR), Internal Hazard Index H_{In}, External Hazard Index H_{Ex}, Annual Gonadal Dose Equivalent (AGDE), Alpha Index I_{α}, and Radioactivity Index I_{γ}, were estimated using their respective models from the literature.

4.1 Calculation of activity concentration in soil samples

All measurements were taken with the samples in contact with the detector housing for 25,200 s, and spectral analysis was performed using Genie 2000 software. The activity concentrations in the measured samples were calculated using Equation 3 [34, 39]:

$$A\,(Bq/kg) = \frac{N_p}{I_{\gamma}\varepsilon Tm} \tag{3}$$

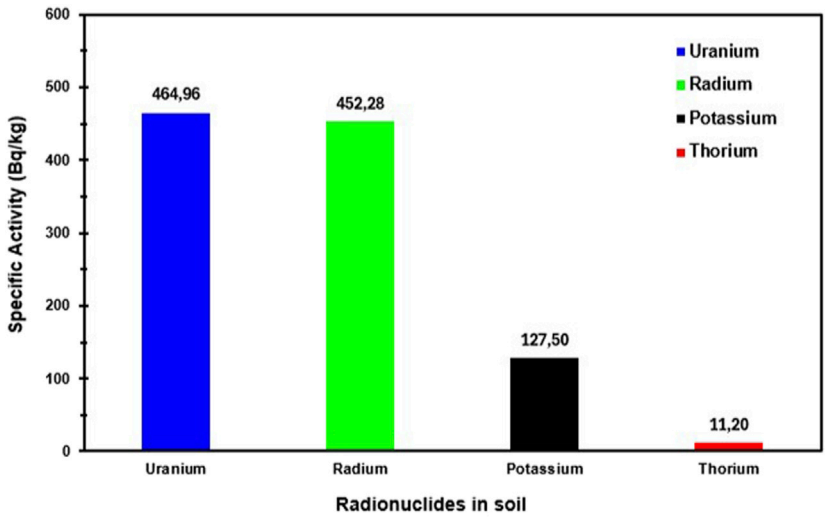

FIGURE 4
The mean specific activity concentration.

TABLE 3 The comparison of radium activity concentration in tailings of different mining wastes.

Tailings type	Min	Max	Mean	References
Phosphate rock Ore	107	1,649	662	[62]
Phosphate Ore	62.3	333.5	253.6	[63]
Phosphate tailings 1	311.0	3,945.8	2,939.0	[64]
Phosphate tailings 2	3,759.8	7,606.3	5,591.2	[64]
Geita gold mine	13 ± 9	99 ± 4	54 ± 3	[65]
Silver mining, zone A	124.26	303.45	200.42	[66]
Silver mining, zone B	105.76	596.26	306.67	[66]
West rand	12.35	941.07	53.09	[23]
Roodepoort	112.02 ± 9.09	1,195.80 ± 30.63	407.41 ± 4.23	This study

Where A (Bq/kg) is the specific activity in a sample, N_p is the activity of the sample with the background activity subtracted.

4.2 The radium equivalent activity Ra_{Eq}

The radium equivalent activity is an index introduced to represent the specific activities of ^{226}Ra, ^{232}Th, and ^{40}K by a single quantity that accounts for the radiation hazards associated with them. The radium equivalent activity was estimated using Equation 4 [5, 39–41]:

$$Ra_{Eq}(Bq/kg) = C_{Ra} + 1.43C_{Th} + 0.077C_K \quad (4)$$

This radiation index uses baseline measurements of 370 Bq/kg for ^{226}Ra, 259 Bq/kg for ^{232}Th, and 4,810 Bq/kg for ^{40}K, as these levels produce equivalent gamma radiation doses [5]. To keep radiation exposure within safe limits, experts recommend that the index should not exceed 370 Bq/kg in soil [42]. This helps to assess how gamma radiation may affect living organisms and allows evaluation of potential health risks in different locations.

4.3 The absorbed dose rate in air (ADR)

The absorbed gamma dose rate measures the rate at which ionizing radiation from gamma rays is deposited at a specific location, providing insight into the potential biological effects of gamma radiation. The total absorbed dose rate due to naturally occurring radioactive materials (NORM) in air 1 m above the ground is calculated using the following equations. Absorbed dose rates are estimated using Equations 5, 6 [40, 43–45]:

TABLE 4 Comparison of radiological health indices with their globally recommended upper limits.

Site	Radiological indices	Minimum	Maximum	Mean	Upper limit
RDP	Ra_{Eq} (Bq/kg)	142.74 ± 9.24	1,242.98 ± 30.78	433.28 ± 17.06	370
	ADR_{Ind} (nGy/h)	114.15 ± 8.51	1,142.21 ± 28.32	397.42 ± 15.17	84
	ADR_{Out} (nGy/h)	57.68 ± 6.40	574.91 ± 14.23	200.35 ± 7.89	59
	$AEDE_{Ind}$ (mSv/y)	0.56 ± 0.04	5.60 ± 0.14	1.95 ± 0.08	0.41
	$AEDE_{Out}$ (mSv/y)	0.07 ± 0.01	0.71 ± 0.02	0.25 ± 0.01	0.07
	$ELCR_{Ind}$ ($\times 10^{-3}$)	1.96 ± 0.15	19.61 ± 0.49	6.82 ± 0.27	1.16
	$ELCR_{Out}$ ($\times 10^{-3}$)	0.25 ± 0.02	2.47 ± 0.06	0.86 ± 0.03	0.29
	H_{In}	0.64 ± 0.06	6.59 ± 0.18	2.27 ± 0.10	≤1
	H_{Ex}	0.34 ± 0.07	3.36 ± 0.12	1.17 ± 0.09	≤1
	AGDE (μSv/y)	388.68 ± 28.75	3,856.56 ± 95.28	1,345.78 ± 52.90	300
	I_γ	0.42 ± 0.04	4.71 ± 0.12	1.46 ± 0.07	≤1
	I_α	0.56 ± 0.05	5.98 ± 0.15	2.04 ± 0.08	<1

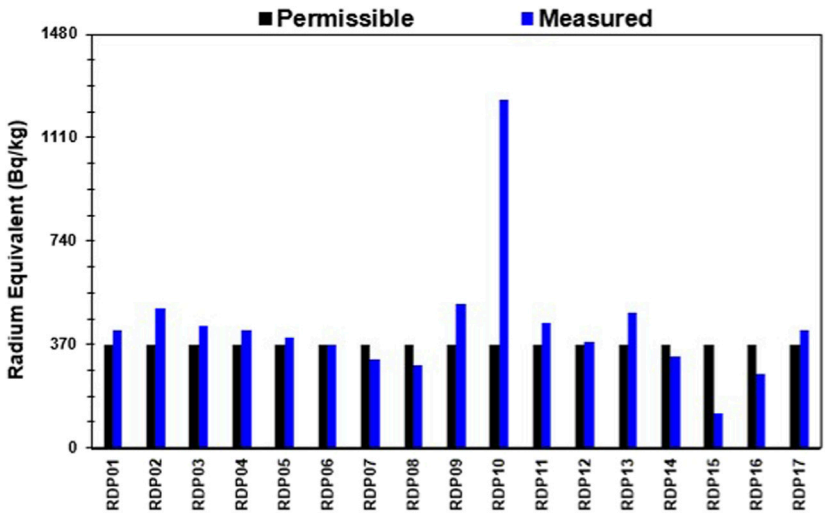

FIGURE 5
The radium equivalent activity in samples.

$$D_{Ind}(nGy/h) = 0.920C_{Ra} + 1.100C_{Th} + 0.0810C_K \quad (5)$$

$$D_{Out}(nGy/h) = 0.462C_{Ra} + 0.604C_{Th} + 0.0417C_K \quad (6)$$

Where 0.462, 0.604, 0.0417, 0.92, 1.1, and 0.081 are dose conversion factors in nGy/h per Bq/kg, and C_{Th}, C_{Ra} and C_K are the radionuclide concentrations for ^{226}Ra, ^{232}Th, and ^{40}K, respectively [5, 41, 46, 47].

4.4 The annual effective dose rate (AEDE)

The air absorbed dose rates found above are multiplied by a conversion factor F with a value of 0.7×10^{-6} Sv/y [5] to convert to the effective dose received by adults and 0.2 and 0.8 for the outdoor and indoor occupancy factors, respectively [46]. The effective dose rate per year should be less than a unity [48]. The indoor and outdoor annual effective dose equivalent is estimated using Equations 7, 8 [5, 49]:

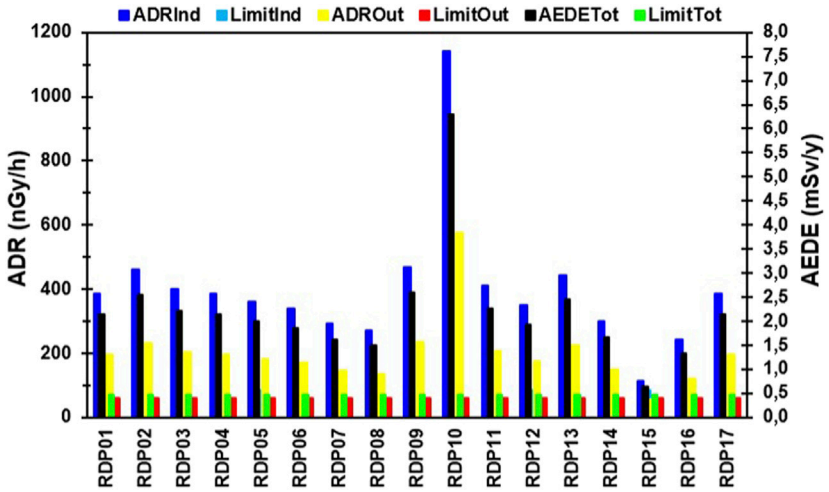

FIGURE 6
The comparison of ADR and AEDE in samples.

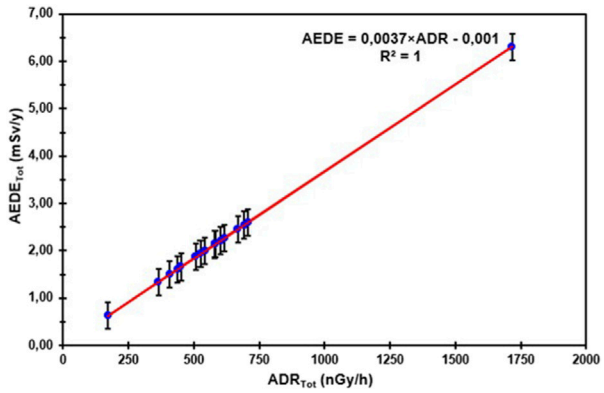

FIGURE 7
The linear plot between ADR and AEDE.

$$AEDE_{Ind}\,(mSv/y) = D_{Ind} \times T \times 0.8 \times F \tag{7}$$

$$AEDE_{Out}\,(mSv/y) = D_{Out} \times T \times 0.2 \times F \tag{8}$$

Where T is hours in a year (365×24 h = 8,760 h), and F is the conversion factor with a value of 0.7×10^{-6} Sv/y.

4.5 The excess lifetime cancer risk (ELCR)

Excess lifetime cancer risk (ELCR) is a term used in radiation protection to estimate the potential increase in a person's cancer risk due to exposure to ionizing radiation that exceeds the baseline risk of cancer exposure without radiation exposure. The indoor and outdoor ELCR values should, on average, be less than or equal to the global average of 1.16×10^{-3} and 0.29×10^{-3}, respectively. The excess lifetime cancer risk $ELCR_{Ind}$ in the indoor environment was calculated using Equation 9 [5, 50–52]:

$$ELCR_{Ind} = AEDE_{Ind} \times DL \times RF \tag{9}$$

The outdoor excess lifetime cancer risk $ELCR_{Out}$ was calculated using Equation 10 [51, 52]:

$$ELCR_{Out} = AEDE_{Out} \times DL \times RF \tag{10}$$

Where DL is the life expectancy, which is about 70 years, and RF is the risk factor, which is given as 0.05 Sv^{-1}. The indoor and outdoor ELCR values should, on average, be less than or equal to the global averages of 1.16×10^{-3} and 0.29×10^{-3}, respectively.

4.6 The internal hazard index H_{In}

The internal hazard index is a crucial concept in radiation protection and safety, assessing potential radiation exposure and hazards linked with radioactive material intake. It establishes tolerable intake limits for radioactive materials and assesses the need for extra precautions like radiation protection or medical follow-up. Inhaling radon and thoron gases can be hazardous to the respiratory organs [53] as these particles undergo alpha decay, thus releasing alpha particles, which can tear the epithelial cells of the lungs, and Equation 11 is used to calculate the hazard index [40, 54–56]:

$$H_{In} = \frac{C_{Ra}}{185} + \frac{C_{Th}}{259} + \frac{C_K}{4810} \tag{11}$$

For the safe use of building materials in shelter construction, the index should be less than one.

4.7 The external hazard index H_{Ex}

External gamma radiation dose refers to the amount of ionising radiation a person is exposed to from gamma rays emitted by an external source, typically associated with radionuclides of concern.

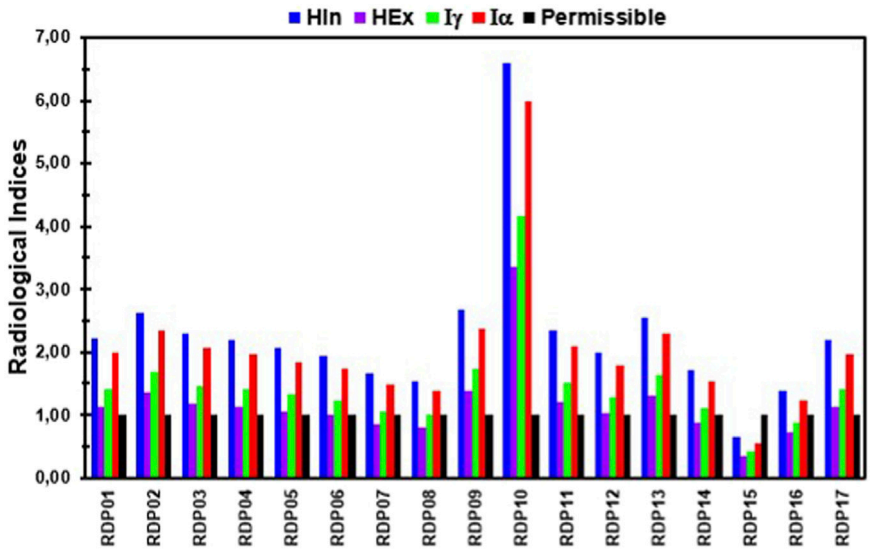

FIGURE 8
The H_{In}, H_{Ex}, I_{γ} and I_{α} indices.

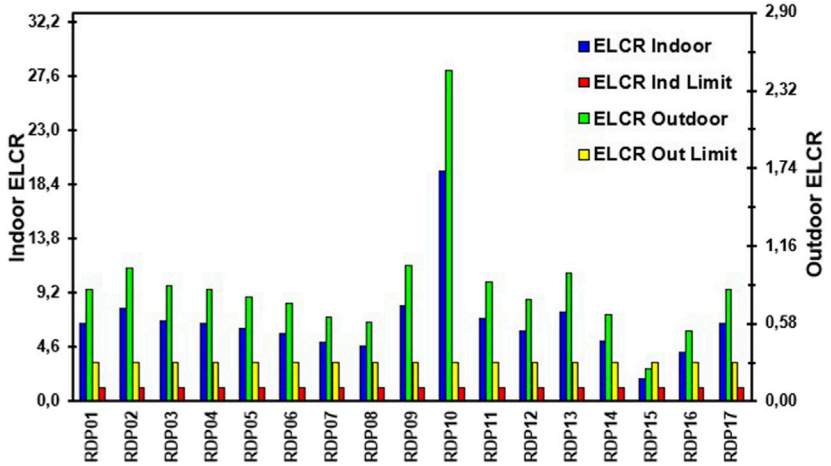

FIGURE 9
The excess lifetime cancer risks and their limits.

To limit this dose, an external hazard index H_{Ex} is calcutaled using Equation 12 [40, 54–57]:

$$H_{Ex} = \frac{C_{Ra}}{370} + \frac{C_{Th}}{259} + \frac{C_K}{4810} \tag{12}$$

For the safety of individuals outdoors, the index should be less than unity.

4.8 The annual gonadal dose equivalent (AGDE)

The annual gonadal dose equivalent (AGDE) is a measure used in radiation protection to estimate the potential dose to the reproductive organs (gonads) from a person's exposure to ionising radiation over a year. The AGDE resulting from the specific activities of ^{226}Ra, ^{232}Th, and ^{40}K was calculated using Equation 13 [40, 58]:

$$AGDE(\mu Sv/y) = 3.09C_{Ra} + 4.18C_{Th} + 0.314C_K \tag{13}$$

The AGDE considers the type of radiation, the amount of radiation exposure, and the sensitivity of the gonads to radiation-induced damage.

4.9 The alpha hazard index I_{α}

The index estimates the risk of internal exposure to alpha radiation from a mixture of α-emitting radionuclides and expresses

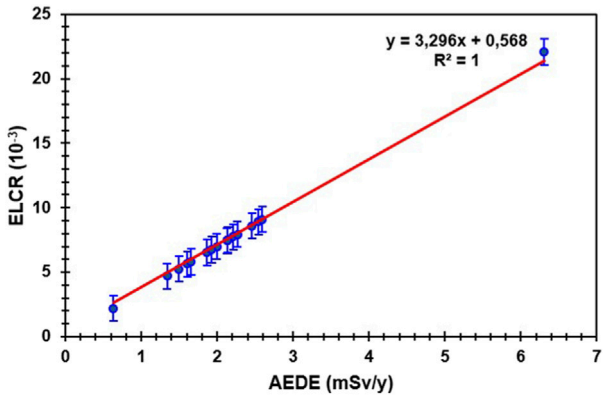

FIGURE 10
The linear plot between ELCR and AEDE.

the total hazard in a single numerical value. Excess alpha radiation from inhalation of radon from building materials is estimated using Equation 14 [12, 59]:

$$I_\alpha = \frac{C_{Ra}}{200} \tag{14}$$

The alpha index, $I_\alpha \leq 1$ is equivalent to 200 Bq/kg of radium. Construction material with ^{226}Ra exceeding 200 Bq/kg should be avoided in building because this may lead to 200 Bq/m^3 of radon, exposing occupants to internal radiation. In the above equations, ^{226}Ra, ^{232}Th, and ^{40}K represent the radionuclide concentrations.

4.10 The radioactivity index I_γ

This study examines the possibility of radiation exposure to human settlements near gold mine tailings dams, especially informal settlements. The plastering sand-like soil can easily be excavated for building purposes, and unaware of its toxicity, people may make bricks and use it as building sand, which will, in turn, expose the inhabitants to gamma radiation. The gamma radiations emitted by certain natural radionuclides in building materials are linked to this index by Equation 15 [50, 51, 60]:

$$I_\gamma = \frac{C_{Ra}}{150} + \frac{C_{Th}}{100} + \frac{C_K}{1500} \tag{15}$$

An increase in the gamma index beyond the worldwide acceptable limit may result in radiation risk, leading to the deformation of human cells, thereby causing cancer. $I_\gamma = 1$ as an upper limit, $I_\gamma \leq 1$ corresponds to 0.3 mSv/y, and $I_\gamma \leq 3$ corresponds to 1 mSv/y. For materials used in bulk like bricks, the ranges of I_γ are: $0.5 \leq I_\gamma \leq 1$ [61].

5 Results and discussion

5.1 Specific activity concentrations of natural radionuclides in samples

Samples from four different gold tailings were collected and analyzed at iThemba LABS. The activity concentration of ^{238}U ranged from 132.88 ± 4.68 to 1,421.46 ± 13.38 with a mean of 464.96 ± 2.08 Bq/kg. The activity concentration of ^{226}Ra ranged from 112.02 ± 9.09 to 1,195.80 ± 30.63 with a mean of 407.42 ± 4.23 Bq/kg, which is 12 the 35 Bq/kg recommended value by [5]. The range of ^{232}Th was from 5.27 ± 0.67 to 19.37 ± 1.98 with a mean of 11.20 ± 1.03 Bq/kg, and ^{40}K activity ranged from 65.23 ± 15.29 to 264.11 ± 25.66 with a mean of 127.50 ± 21.85 Bq/kg as presented in Table 2. The ^{238}U was calculated from the concentrations of ^{214}Pb and ^{214}Bi, while radium was calculated from its signal of 186.20 keV. The findings showed that ^{238}U and ^{226}Ra activity exceeded the global average of 30 and 35 Bq/kg, respectively, while ^{232}Th and ^{40}K were below their respective limits [5].

The concentration of ^{40}K ranged from 113.34 ± 20.80 Bq/kg to 145.79 ± 22.51 Bq/kg with a mean of 126.15 ± 10.90 Bq/kg, which is 11 times the concentration of ^{232}Th. The level of ^{40}K is below the permissible limit of 400 Bq/kg, and ^{232}Th ranged from 8.25 ± 1.31 to 11.20 ± 1.03 Bq/kg with a mean of 10.06 ± 0.68 Bq/kg. The mean concentration of ^{226}Ra is 40.3 times that of ^{232}Th, whereas it is 3.5 times the level of ^{40}K in the samples, and in decreasing order they are: ^{238}U > ^{226}Ra > ^{40}K > ^{232}Th.

In this analysis, ^{214}Bi and ^{214}Pb were used to estimate ^{238}U, assuming secular equilibrium [29, 30], and radium was estimated directly from its 186 keV signal, as there were very few significant responses from ^{235}U signals to indicate its presence. Both ^{214}Bi and ^{214}Pb are short-lived decay products of textsuperscript222Rn gas and are strong gamma-ray emitters. Their characteristic gamma rays—295 and 351.9 keV for ^{214}Pb, and 609.3, 1,120.3, and 1764.5 keV for ^{214}Bi–are easily detected by γ-ray spectrometry.

The use of these daughter products to determine the parent uranium concentration relies on the concept of secular equilibrium, which states that the activity of each intermediate product is proportional to the amount of uranium present because its rate of decay equals its rate of production. The activities of ^{226}Ra and ^{214}Pb were correlated to see if the analysis was indeed carried out at radioactive secular equilibrium samples for Roodepoort tailings. There was a good positive correlation between the activities of ^{226}Ra and ^{238}U in the samples, indicating the system was indeed at radioactive secular equilibrium for the Roodepoort tailings samples after 42 days.

The activity concentration of ^{232}Th was detected, but it was within the background levels. The activity concentration of ^{40}K was present at an intermediate level but below the permissible limit of 400 Bq/kg [5]. The specific activity concentration of ^{238}U and ^{226}Ra dominated all NORM activities in the soil samples from Roodepoort tailings, as shown in Figure 4.

Table 3 compares radium in this study, in the region, and globally in tailings of different mined resources. The high radium activity concentrations, compared with activities in other tailings except for gold from various countries, are presented in Table 3. The mean radium concentration in the CMR gold tailings is 451 ± 8.00 Bq/kg, which is lower than the 662 Bq/kg found in New Zealand's phosphate rock ore [62], but higher than the 253.6 Bq/kg in Saudi Arabia's phosphate ore [63]. Compared to phosphate tailings in Tanzania, which exceed 2,939.0 and 5,591.2 Bq/kg [64], the CMR concentration is significantly lower. However, it is higher than the concentration of 54 ± 3 Bq/kg around the Geita Gold Mine in Tanzania [65], and higher than 200.42 and 306.67 Bq/kg in silver mining areas of Brazil [66]. It is notable that phosphate rock

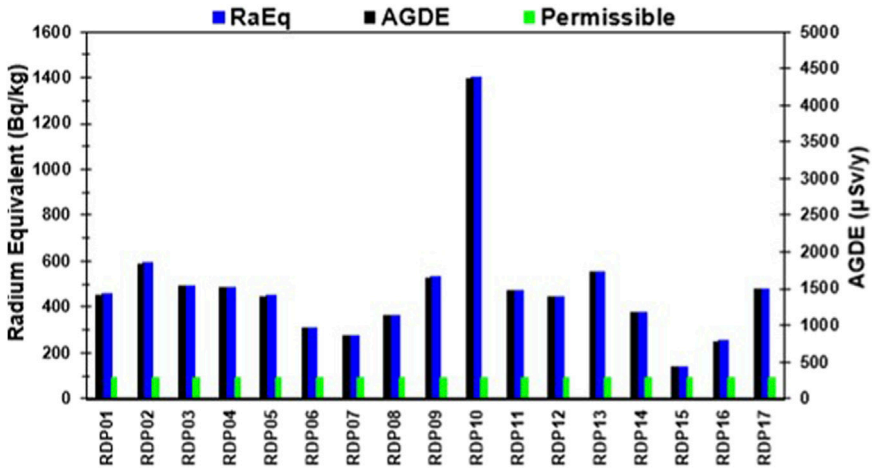

FIGURE 11
The AGDE and Rad_{Eq} in Roodepoort samples.

waste have high radium and uranium activities. This is because the fertilizer processing focuses solely on extracting phosphates, leaving uranium concentrated in the waste.

5.2 Radiological hazard assessment in soil samples

For RDP samples shown in Table 4, the Ra_{Eq} has a mean of 433.28 ± 17.06 Bq/kg, a value 1.2 times the permissible limit of 370 Bq/kg [42]. The indoor and outdoor air absorbed dose rates have average values which exceeded their recommended values of 84 and 59 nGy/h, respectively. The indoor and outdoor AEDE are above their recommended values of 0.41 and 0.07 mSv/y, respectively [5, 67]. The values of the AEDE are higher than 0.23 ± 10.07 mSv/y for outdoor and 0.92 ± 10.29 mSv/y for indoor, as reported in a study in Cameroon [68]. Both the cancer risks (ELCR) are higher than their recommended values of 1.16×10^{-3} and 0.29×10^{-3}, respectively [67].

The internal hazard index is 2.51 times higher than its recommended value, while the external hazard index is 1.3 times higher than its recommended value but is of the same order as the value found in the study in Cameroon [68] and higher than the value of 0.59 reported in Turkey [69]. The mean values of AGDE, I_α, and I_γ are 4.5, 2.0, and 1.5 times higher than their recommended values, respectively, and the average I_γ is lower than the value of 1.60 reported in Turkey [69].

In the figure, the radium equivalent activity of the RDP gold tailings samples shows that only 4 out of 17 samples–RDP 06, 07, 15, and 16—with RDP 15 having the lowest values, fall below the recommended regulatory benchmark of 370 Bq/kg [42, 70], which corresponds to an external dose rate limit of about 1.5 mSv/y [70] for shelter occupants. The RDP samples with high radium levels–RDP 02, 03, 04, 05, 09, 10, 11, 12, 13, and 17—showed high Ra_{Eq} values, with RDP 10 having the highest value, as shown in Figure 5; overall, the values exceeded the recommended limit. The mean radium equivalent was higher than the 189 Bq/kg found in a study of tailings in Tanzania [65].

The relationship between the ADR and AEDE in Roodepoort gold tailings samples is shown in Figure 6. The internal and external absorbed dose rates exceeded their recommended limits of 84 and 59.9 nGy/h, respectively [5]. The indoor ADR is similar to the 413.50 nGy/h reported in the West Rand [23], but higher than the value found in Cameroon, which was 188.2 ± 59.4 nGy/h.The outdoor ADR is higher than 49.09 nGy/h and 70.12 nGy/h, which were found in the East Rand and Soweto, respectively [23]. The total annual effective dose equivalent exceeded the permitted value of 0.48 mSv/y in all samples, and they were higher than the global limit of 1.00 mSv/y [5, 71], and they were higher than the values in the East Rand of 0.51 mSv/y [23]. Figure 6 shows that a proportionality exists between the absorbed dose rate and the annual effective dose rate.

It is evident in Figure 6 that all samples follow a similar distribution trend to the absorbed dose rate, as the annual effective dose has a linear relationship with the absorbed dose rate. The relationship between ADR and AEDE in Roodepoort gold tailings samples is illustrated. The annual effective dose equivalent increases with an increase in the air absorbed dose rate; this relationship is confirmed by Figure 7, which shows that a proportionality exists between the absorbed dose rate and the annual effective dose rate.

The radiological health indices in the Roodepoort gold tailings, for which the permissible maximum value should be unity, are shown in Figure 8, with RDP 10 exceeding all others and RDP 15 having the lowest values in H_{In}, H_{Ex}, I_γ, and I_α. These indicators suggest that, in the long term, people who reside permanently in these areas may face health issues.

Figure 9 shows a comparison of indoor and outdoor excess lifetime cancer risk factors calculated for these samples. For Sample RDP 10, the outdoor ELCR is nine times higher than its acceptable value. Both the indoor and outdoor ELCR exceed their respective limits of 1.16×10^{-3} and 0.29×10^{-3} [5, 67], as shown in the figure below.

Figure 10 shows a plot of the ELCR and AEDE values for the gold tailings soil samples from Roodepoort. This plot indicates a

linear relationship between radiation exposure and the likelihood of developing cancer during a human lifetime.

Figure 11 shows the relationship between the radium equivalent activity and the annual gonadal dose equivalent in the tailings samples from Roodepoort. The graph indicates that the AGDE is proportional to the activity present in the samples. The mean AGDE is 1,345.78 ± 52.90 μSv/y, which is 4.5 times the recommended value of 300 μSv/y [72] and is higher than the AGDE value of 678 μSv/y found in a study in Tanzania [65].

Soil samples with high activity tend to release high levels of radiation; therefore, all radiation hazard indices for these samples are high, and the reproductive organs (gonads) of people exposed to such soil are at risk of significant radiation exposure, which can affect future generations. Radiation can cause genetic damage in the gonads, leading to mutations and hereditary diseases, as there is no minimum safe dose of radiation to the gonads [73]. No amount of ionizing radiation is considered negligible, as it is believed that any exposure may increase the risk of stochastic effects. It is assumed that these effects follow a linear model with no specific threshold; therefore, radiology specialists encourage adherence to the ALARA principle [74].

As radiation is invisible to the human eye but can be harmful at high levels, it is important to keep exposure as low as possible. The ALARA principle consists of three factors: time, distance, and shielding. If citizens live permanently near radioactive waste, these ALARA factors are continuously disregarded, which also violates the United Nations Sustainable Development Goals (SDGs), such as SDG 3: Good Health and Wellbeing and SDG 11: Sustainable Cities and Communities. If such radiation reaches water bodies, both SDG 14: Life Below Water and SDG 15: Life on Land are also not observed of [75].

6 Conclusion and outlook

The Roodepoort gold tailings samples were collected, prepared, and analyzed for radioactivity using a high-energy resolution coaxial HPGe γ - detector. In this analysis, both uranium and radium exceeded their recommended global limits, while thorium and potassium were below their recommended limits.

The average radium equivalent was 1.2 times higher than its recommended value of 370 Bq/kg. The average indoor and outdoor absorbed dose rates were 4.7 and 3.3 times higher than their respective recommended values of 84 nGy/h and 59 nGy/h. The average indoor and outdoor annual effective dose equivalents were 4.8 and 3.6 times higher than their recommended values of 0.41 and 0.07 mSv/y, respectively. The average indoor and outdoor excess lifetime cancer risks were 5.9 and 3.0 times higher than their respective recommended values of 1.16×10^{-3} and 0.29×10^{-3}. The averages of internal and external hazard indices were 2.5 and 1.3 times higher than unity. The annual gonadal dose equivalent had a mean value 4.5 times higher than the recommended value of 300 μSv/y. The mean values of the alpha and gamma hazard indexes were 2.26 and 1.61 times greater than unity, respectively.

Although they originate from background ionising radiation, these findings may, in the long term, have deleterious health effects on residents in the vicinity of the tailings, as the recommended radiological health limits were exceeded. Additional oversight and regulatory control measures are required to ensure the safety of the environment and residents near the tailings. Our study was limited to measuring radioactivity using gamma spectroscopy and did not use alpha spectroscopy, even though radon gas is also an alpha emitter. Future studies may address this aspect.

Data availability statement

The original contributions presented in the study are included in the article/supplementary material, further inquiries can be directed to the corresponding author.

Author contributions

MM: Writing – original draft, Writing – review and editing. SN: Funding acquisition, Supervision, Writing – review and editing. SM: Funding acquisition, Supervision, Writing – review and editing. BK: Supervision, Writing – review and editing. PLM: Supervision, Writing – review and editing. PPM: Supervision, Writing – review and editing.

Funding

The author(s) declared that financial support was received for this work and/or its publication. This research was funded by the National Research Foundation (NRF) of South Africa under grant number CPRR23040388976.

Acknowledgements

The first author thanks the NRF-iThemba LABS for providing access to the facility. Special thanks are extended to Mr. A. Kwelilanga, an applied nuclear and radiation physicist at iThemba LABS, for his knowledge of gamma spectrometric analysis. Most importantly, the Department of Physics, University of Zululand, supported this study.

Conflict of interest

The author(s) declared that this work was conducted in the absence of any commercial or financial relationships that could be construed as a potential conflict of interest.

Generative AI statement

The author(s) declared that generative AI was not used in the creation of this manuscript.

Any alternative text (alt text) provided alongside figures in this article has been generated by Frontiers with the support of artificial intelligence and reasonable efforts have been made to ensure accuracy, including review by the authors wherever possible. If you identify any issues, please contact us.

Publisher's note

References

1. Mouandza SL, Moubissi A, Abiama P, Ekogo T, Ben-Bolie G. Study of natural radioactivity to assess radiation hazards from soil samples collected from mounana in the south-east of gabon. *Int J Radiat Res* (2018) 16:443–53. doi:10.18869/acadpub.ijrr.16.4.443

2. Chaturvedi A, Jain V. Effect of ionizing radiation on human health. *Int Journal Plant Environ* (2019) 5:200–5. doi:10.18811/ijpen.v5i03.8

3. Sarangi A. Uranium and its measurement in ore by radiometric method. *J Mines, Met Fuels* (2000).

4. Willis R *Presidential address: the uranium story-an update*, 106. Johannesburg: Southern African Institute of Mining and Metallurgy (2006). p. 601–9.

5. Unscear S. *Effects of ionising radiation*. New York: United Nations (2000). p. 453–87.

6. Mehra R. Use of gamma ray spectroscopy measurements for assessment of the average effective dose from the analysis of 226ra, 232th, and 40k in soil samples. *Indoor Built Environ* (2009) 18:270–5. doi:10.1177/1420326x09104140

7. Cruz-Nova P, Trujillo-Nolasco M, Aranda-Lara L, Ferro-Flores G, García BO. Radiobiological effect of alpha particles. The scientific basis of targeted alpha-particle therapy. *Nucl Med Biol* (2025) 146-147:109044. doi:10.1016/j.nucmedbio.2025.109044

8. Klotz L-O, Steinbrenner H. Cellular adaptation to xenobiotics: interplay between xenosensors, reactive oxygen species and foxo transcription factors. *Redox Biology* (2017) 13:646–54. doi:10.1016/j.redox.2017.07.015

9. Trujillo-Nolasco M, Morales-Avila E, Cruz-Nova P, Katti KV, Ocampo-García B. Nanoradiopharmaceuticals based on alpha emitters: recent developments for medical applications. *Pharmaceutics* (2021) 13:1123. doi:10.3390/pharmaceutics13081123

10. Pizzino G, Irrera N, Cucinotta M, Pallio G, Mannino F, Arcoraci V, et al. Oxidative stress: harms and benefits for human health. *Oxidative Medicine Cellular Longevity* (2017) 2017:8416763. doi:10.1155/2017/8416763

11. Kamunda C, Mathuthu M, Madhuku M. An assessment of radiological hazards from gold mine tailings in the province of gauteng in South Africa. *Int J Environ Res Public Health* (2016) 13:138. doi:10.3390/ijerph13010138

12. Stoulos S, Manolopoulou M, Papastefanou C. Assessment of natural radiation exposure and radon exhalation from building materials in greece. *J Environ Radioactivity* (2003) 69:225–40. doi:10.1016/S0265-931X(03)00081-X

13. National Research Council (US) Committee on Health Risks of Exposure to Radon (BEIR VI). *Health effects of exposure to radon: BEIR VI*, 6. Washington, DC: National Academies Press (1999).

14. Kovler K, Friedmann H, Michalik B, Schroeyers W, Tsapalov A, Antropov S, et al. Basic aspects of natural radioactivity. In: *Naturally occurring radioactive materials in construction (Elsevier)* (2017). p. 13–36.

15. Chanda-Kapata P. Public health and mining in east and Southern Africa: a desk review of the evidence. *Zambia Ministry Health Train Res Support Centre Reg Netw Equity Health East South Africa (Equinet)* (2020).

16. Zivuku M, Kgabi NA, Tshivhase VM. Assessment of radioactivity in particulate matter and soil from selected mining towns of erongo region, Namibia. *Scientific Afr* (2023) 20:e01722. doi:10.1016/j.sciaf.2023.e01722

17. Winde F. Uranium pollution of the wonderfonteinspruit, 1997-2008 part 1: uranium toxicity, regional background and mining-related sources of uranium pollution. *Water Sa* (2010) 36:239–56.

18. Laker MC. Environmental impacts of gold mining—with special reference to South Africa. *Mining* (2023) 3:205–20. doi:10.3390/mining3020012

19. Nkosi V, Wichmann J, Voyi K. Chronic respiratory disease among the elderly in South Africa: any association with proximity to mine dumps? *Environ Health* (2015) 14:33. doi:10.1186/s12940-015-0018-7

20. Mpanza M, Adam E, Moolla R. Perceptions of external costs of dust fallout from gold mine tailings: west wits basin. *Clean Air J* (2020) 30:1–12. doi:10.17159/caj/2020/30/1.7566

21. Dragović S, Janković L, Onjia A. Assessment of gamma dose rates from terrestrial exposure in serbia and montenegro. *Radiat Protection Dosimetry* (2006) 121:297–302. doi:10.1093/rpd/ncl099

22. Mohuba SC, Abiye T, Nhleko S. Evaluation of radionuclide levels in drinking water from communities near active and abandoned gold mines and tailings in the west rand region, gauteng, South Africa. *Minerals* (2022) 12:1370. doi:10.3390/min12111370

23. Moshupya PM, Mohuba SC, Abiye TA, Korir I, Nhleko S, Mkhosi M. *In situ* determination of radioactivity levels and radiological doses in and around the gold mine tailing dams, gauteng province, South Africa. *Minerals* (2022) 12:1295. doi:10.3390/min12101295

24. Naicker K, Cukrowska E, McCarthy T. Acid mine drainage arising from gold mining activity in johannesburg, South Africa and environs. *Environ Pollution* (2003) 122:29–40. doi:10.1016/s0269-7491(02)00281-6

25. Tutu H, Cukrowska EM, McCarthy TS, Hart R, Chimuka L. Radioactive disequilibrium and geochemical modelling as evidence of uranium leaching from gold tailings dumps in the witwatersrand basin. *Int J Environ Anal Chem* (2009) 89:687–703. doi:10.1080/03067310902968749

26. Viljoen M. The life, death and revival of the central rand goldfield. *World Gold Conf* (2009) 2009:131–8.

27. Salvador F, Marchais T, Pérot B, Allinei P-G, Morales F, Gueton O, et al. Gamma-ray spectroscopy for the characterization of uranium contamination in nuclear decommissioning. In: *EPJ web of conferences*. Les Ulis, France: EDP Sciences (2023) 288.

28. Ion A, Cosac A, Ene VV. Natural radioactivity in soil and radiological risk assessment in lişava uranium mining sector, banat mountains, Romania. *Appl Sci* (2022) 12:12363. doi:10.3390/app122312363

29. Kareem AA, Hady HN, Abojassim AA. Measurement of natural radioactivity in selected samples of medical plants in Iraq. *Int J Phys Sci* (2016) 11:178–82. doi:10.5897/ijps2016.4507

30. Najam LA, Younis SA. Assessment of natural radioactivity level in soil samples for selected regions in nineveh province (iraq). *Int J Novel Res Phys Chem and Mathematics* (2015) 2:1–9.

31. Bezuidenhout J. Measuring naturally occurring uranium in soil and minerals by analysing the 352 kev gamma-ray peak of 214pb using a nai (tl)-detector. *Appl Radiat Isot* (2013) 80:1–6. doi:10.1016/j.apradiso.2013.05.008

32. Gyuk P, Habila S, Dogara M, Kure N, Daniel H, Handan T. Determination of radioactivity levels in soil samples at chikun environment of kaduna metropolis using gamma ray spectrometry. *Sci World J* (2017) 12:52–5.

33. Becegato VA, Ferreira FJF, Machado WCP. Concentration of radioactive elements (u, th and k) derived from phosphatic fertilizers in cultivated soils. *Braz Arch Biol Technology* (2008) 51:1255–66. doi:10.1590/s1516-89132008000600022

34. Tzortzis M, Tsertos H, Christofides S, Christodoulides G. Gamma-ray measurements of naturally occurring radioactive samples from cyprus characteristic geological rocks. *Radiat Measurements* (2003) 37:221–9. doi:10.1016/s1350-4487(03)00028-3

35. Masok F, Masiteng P, Mavunda R, Maleka P, Winkler H. Measurement of radioactivity concentration in soil samples around phosphate rock storage facility in richards bay, South Africa. *J Radiation Research Applied Sciences* (2018) 11:29–36. doi:10.1016/j.jrras.2017.10.006

36. Barescut J, Hlatshwayo I, Lindsay R, Ndwandwe O, Newman R. *In-situ* gamma-ray mapping of environmental radioactivity at ithemba labs and associated risk assessment. *Radioprotection* (2009) 44:825–30. doi:10.1051/radiopro/20095147

37. Gray P, Ahmad A. Linear classes of ge (li) detector efficiency functions. *Nucl Instr Methods Phys Res Section A: Acc Spectrometers, Detectors Associated Equipment* (1985) 237:577–89. doi:10.1016/0168-9002(85)91069-1

38. Bhattacharyaa T, Nagaiahb N, Reddya BRM, Sharmac P. Monte carlo calculation of the efficiency calibration curve for hpge detectors. *Indian J Pure and Appl Phys* (2018) 56:628–30.

39. Khandaker MU, Jojo PJ, Kassim HA. Determination of primordial radionuclides in natural samples using hpge gamma-ray spectrometry. *APCBEE Proced* (2012) 1:187–92. doi:10.1016/j.apcbee.2012.03.030

40. Agbalagba EO, Oghenevovwero Emmanuel E. Occupational and public risk assessment of norms in soil of the niger delta region of nigeria after six decades of hydrocarbon exploitation. *Arabian J Geosciences* (2023) 16:328. doi:10.1007/s12517-022-11151-w

41. Uosif M *Specific activity of 226ra, 232th and 40k for assessment of radiation hazards from building materials commonly used in upper Egypt*, 6. Isparta, Tukey: Süleyman Demirel University (2011). p. 120–6.

42. Nea-Oecd N. *Exposure to radiation from natural radioactivity in building materials*. Boulogne-Billancourt, France: NEA (1979).

43. Imani M, Adelikhah M, Shahrokhi A, Azimpour G, Yadollahi A, Kocsis E, et al. Natural radioactivity and radiological risks of common building materials used in semnan province dwellings, Iran. *Environ Sci Pollut Res* (2021) 28:41492–503. doi:10.1007/s11356-021-13469-6

44. Sahu S, Bhangare R, Ajmal P, Pandit G. Evaluation of the radiation dose due to the use of fly ash from thermal power plants as a building material. *Radioprotection* (2016) 51:135–40. doi:10.1051/radiopro/2016018

45. Unscear S. *Sources and effects of ionizing radiation, unscear 2008 report*. United Nations Scientific Committee on the Effects of Atomic Radiation (2008).

46. Hameed PS, Pillai GS, Mathiyarasu R. A study on the impact of phosphate fertilizers on the radioactivity profile of cultivated soils in srirangam (tamil nadu, India). *J Radiat Res Appl Sci* (2014) 7:463–71. doi:10.1016/j.jrras.2014.08.011

47. Fávaro D. Natural radioactivity in phosphate rock, phosphogypsum and phosphate fertilizers in Brazil. *J Radioanal Nucl Chem* (2005) 264:445–8. doi:10.1007/s10967-005-0735-4

48. Mohammed NK, Mazunga MS. Natural radioactivity in soil and water from likuyu village in the neighbourhood of mkuju uranium deposit. *Int J Anal Chem* (2013) 2013:501856. doi:10.1155/2013/501856

49. Dina NT, Das SC, Kabir MZ, Rasul MG, Deeba F, Rajib M, et al. Natural radioactivity and its radiological implications from soils and rocks in jaintiapur area, north-east Bangladesh. *J Radioanal Nucl Chem* (2022) 331:4457–68. doi:10.1007/s10967-022-08562-0

50. Akpanowo M, Umaru I, Iyakwari S, Joshua EO, Yusuf S, Ekong GB. Determination of natural radioactivity levels and radiological hazards in environmental samples from artisanal mining sites of anka, north-west Nigeria. *Scientific Afr* (2020) 10:e00561. doi:10.1016/j.sciaf.2020.e00561

51. Aguko WO, Kinyua R, Githiri JG. Natural radioactivity and excess lifetime cancer risk associated with soil in kargi area, Marsabit-Kenya. *J Geosci Environ Prot* (2020) 8:127–43. doi:10.4236/gep.2020.812008

52. Taskin H, Karavus M, Ay P, Topuzoglu A, Hidiroglu S, Karahan G. Radionuclide concentrations in soil and lifetime cancer risk due to gamma radioactivity in kirklareli, Turkey. *J Environ Radioactivity* (2009) 100:49–53. doi:10.1016/j.jenvrad.2008.10.012

53. Righi S, Bruzzi L. Natural radioactivity and radon exhalation in building materials used in italian dwellings. *J Environ Radioactivity* (2006) 88:158–70. doi:10.1016/j.jenvrad.2006.01.009

54. Echeweozo E. Evaluation of activity concentration of 40 k, 226ra and 232th and radiological hazards in commercial wall paints used in Nigeria. *Polytechnica* (2022) 5:13–20. doi:10.1007/s41050-022-00037-1

55. Osimobi J, Avwiri G, Agbalagba E. Radiometric and radiogenic heat evaluation of natural radioactivity in soil around solid minerals mining environment in south-eastern Nigeria. *Environ Process* (2018) 5:859–77. doi:10.1007/s40710-018-0336-1

56. Raghu Y, Harikrishnan N, Chandrasekaran A, Ravisankar R. Assessment of natural radioactivity and associated radiation hazards in some building materials used in kilpenathur, tiruvannamalai dist, tamilnadu, India. *AIP Conf Proc* (2015) 1675:020047. doi:10.1063/1.4929205

57. Kumar A, Kumar M, Singh B, Singh S. Natural activities of 238u, 232th and 40k in some indian building materials. *Radiat Measurements* (2003) 36:465–9. doi:10.1016/s1350-4487(03)00173-2

58. Tufail M. Radium equivalent activity in the light of unscear report. *Environ Monitoring Assessment* (2012) 184:5663–7. doi:10.1007/s10661-011-2370-6

59. Al-Hwaiti M, Al-Khashman O, Al-Khateeb L, Freig F. Radiological hazard assessment for building materials incorporating phosphogypsum made using eshidiya mine rock in Jordan. *Environ Earth Sci* (2014) 71:2257–66. doi:10.1007/s12665-013-2629-z

60. Roselin MSU, Shanthi G. Study of gross alpha and gross beta activities in rock samples of western ghats in kanyakumari district. *Int J Appl Sci* (2016) 5:1–5. doi:10.21013/jas.v5.n1.p1

61. Turhan Ş, Gündüz L. Determination of specific activity of 226ra, 232th and 40k for assessment of radiation hazards from turkish pumice samples. *J Environ Radioactivity* (2008) 99:332–42. doi:10.1016/j.jenvrad.2007.08.022

62. Pearson AJ, Gaw S, Hermanspahn N, Glover CN, Anderson CW. Radium in New Zealand agricultural soils: phosphate fertiliser inputs, soil activity concentrations and fractionation profiles. *J Environ Radioactivity* (2019) 205:119–26. doi:10.1016/j.jenvrad.2019.05.010

63. Nassef M, Qutub M, Fallatah O, Alyami J, Natto HD, Yahay A. Determination of radioactivity concentrations in phosphate ore and fertilizer to assess their radiological impacts using gamma spectrometry technique in Saudi Arabia. *Environ Monit Assess* (2025) 197:1–13. doi:10.1007/s10661-025-14606-1

64. Mdachi DD, Rugaika AM, Machunda RL. The assessment of heavy metals and natural radioactivity in the phosphate tailings at minjingu mines in Tanzania. *J Ecol Eng* (2024) 25:269–77. doi:10.12911/22998993/175249

65. Mwimanzi JM, Haneklaus NH, Bituh T, Brink H, Kiegiel K, Lolila F, et al. Radioactivity distribution in soil, rock and tailings at the geita gold mine in Tanzania. *J Radiat Res Appl Sci* (2025) 18:101528. doi:10.1016/j.jrras.2025.101528

66. Escareño-Juarez E, Fernández-Saavedra R, Gómez-Mancebo MB, Barrado AI, Cardona AI, Rucandio I. Radioactivity levels and heavy metal concentration in mining areas in zacatecas, Mexico. *Toxics* (2024) 12:818. doi:10.3390/toxics12110818

67. Qureshi AA, Tariq S, Din KU, Manzoor S, Calligaris C, Waheed A. Evaluation of excessive lifetime cancer risk due to natural radioactivity in the rivers' sediments of northern Pakistan. *J Radiat Res Appl Sci* (2014) 7:438–47. doi:10.1016/j.jrras.2014.07.008

68. Nguelem EJM, Ndontchueng MM, Motapon O. Determination of 226ra, 232th, 40k, 235u and 238u activity concentration and public dose assessment in soil samples from bauxite core deposits in western Cameroon. *SpringerPlus* (2016) 5:1253. doi:10.1186/s40064-016-2895-9

69. Dizman S, Görür FK, Keser R. Determination of radioactivity levels of soil samples and the excess of lifetime cancer risk in rize province, Turkey. *Int J Radiat Res* (2016) 14:237. doi:10.18869/acadpub.ijrr.14.3.237

70. Madruga M, Miró C, Reis M, Silva L. Radiation exposure from natural radionuclides in building materials. *Radiat Prot Dosimetry* (2019) 185:49–57. doi:10.1093/rpd/ncy256

71. Agency IAE. *Radiation protection and safety of radiation sources: international basic safety standards*. Vienna, Austria: International Atomic Energy Agency (2014).

72. Maglas NN, Turki SA, Qiang Z, Ali MM, Osta AA, Alwarqi MS, et al. Assessment of radioactive nuclides and heavy metals in soil and drinking water in lahij city, Yemen. *Appl Radiat Isot* (2025) 215:111566. doi:10.1016/j.apradiso.2024.111566

73. Doolan A, Brennan PC, Rainford LA, Healy J. Gonad protection for the antero-posterior projection of the pelvis in diagnostic radiography in dublin hospitals. *Radiography* (2004) 10:15–21. doi:10.1016/j.radi.2003.12.002

74. Hemalatha A, Chougule A, Athiyaman M, Joan M, Kumar H, Sharma N. Poster. *J Med Phys* (2018) 43:S39–S111.

75. Economic D. *The sustainable development goals report 2020*. Virginia: Stylus Publishing, LLC (2020).